Fusion Engineering and Design 202 (2024) 114362

Contents lists available at ScienceDirect

Fusion Engineering and Design

journal homepage: www.elsevier.com/locate/fusengdes

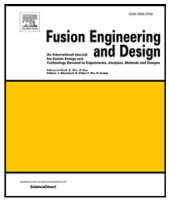

An OpenFOAM multi-region solver for tritium transport modeling in fusion systems

Federico Hattab *, Simone Siriano, Fabio Giannetti

Nuclear Engineering Research Group, DIAEE - Sapienza University of Rome, Corso Vittorio Emanuele II 244, 00186 Rome, Italy

ARTICLE INFO

Keywords:
Hydrogen
Membranes
OpenFOAM
Permeation
Tritium transport

ABSTRACT

The transport, permeation and retention of tritium inside nuclear fusion reactors is a topic of great interest due to the scarcity of the isotope, its ease of diffusion through materials and its radioactivity. An accurate balance of tritium is needed in all the fuel cycle, and each loss term needs to be evaluated in detail. In this context, reliable and flexible tools to evaluate tritium permeation and retention are a necessity for the development of fusion technologies. This work presents the OpenFOAM `PermeAtion Solver for Tritium Analysis Foam` (`pastaFoam`) solver and two custom boundary conditions, along with a series of verification and validation cases. The solver inherits all capabilities of the base solver, `chtMultiRegionFoam`, and is capable to simulate hydrogen transport in coupled fluid–solid systems in the presence of hydrogen traps, under diffusion limited regime or accounting for surface effects. All features are tested against analytical solutions and results are compared with other tritium transport codes. Agreement with experimental data is aligned with results of numerical benchmarks from literature.

1. Introduction

Current efforts in the development of thermonuclear fusion power plants are directed towards deuterium (D) - tritium (T) reaction-based machines, and see T as a fundamental element required to fuel the reaction. Due to the scarce natural abundance of T and its limited man-made supply, fusion devices need to be self-sufficient and produce the isotope themselves, in the Breeding Blanket (BB). For instance, the Affordable, Robust and Compact (ARC) reactor design uses a liquid immersion BB made of FLiBe molten salt, that acts as coolant, shield and tritium breeder [1–3]. Tritium is produced mainly via reaction of neutrons with Li^6, while beryllium acts as a neutron multiplier. Other concepts such as the EU DEMO HCPB BB [4], the CFETR HCPB BB [5] and the K-DEMO blanket [6] use a solid breeder in the form of pebble beds, while the EU WCLL BB [7] and the CFETR COOL BB [8] concepts use liquid PbLi flowing inside dedicated components. The isotope is hazardous due to its radioactivity and it is the main source term during normal operation and in case of accidental events. Thus, strict accountancy is required to ensure compliance with regulatory limits and guarantee self-sustaining operation through efficient recycling.

For these reasons, but also to aid the design of critical components, reliable numerical tools for tritium transport are needed. Several codes and models have been developed during the years [9–16]. The 1D system-level Tritium Migration Analysis Program (TMAP) is considered the reference application for safety analyses. Version 4 and 7 of the code have been widely used [17,18], and its latest version, TMAP8, is currently under development at Idaho National Laboratory (INL) [19,20]. Other developments have also mainly focused on a system-level approach or on finite-element methods.

A component-level approach can give useful insight on the behavior of geometrically complex systems with complicated thermal/fluid conditions, and is a natural complement to the system-level approach. In this work a Computational Fluid Dynamics (CFD) tritium transport model developed by the Nuclear Engineering Research Group (NERG) of Sapienza University of Rome is presented. The numerical solver is based on the OpenFOAM (OF) open-source CFD toolbox. The model was used to study a Double Wall Heat eXchanger (DWHX) for an ARC-like reactor [21], to address concerns regarding hydrogen transport through the hot and thin walls of the component. Modeling work of tritium transport using OF has been done, with a different development approach compared to the present work, by [14] in the framework of the EUROfusion Consortium. The solver presented in this work, named `PermeAtion Solver for Tritium Analysis Foam (pastaFoam)`, inherits all the capabilities of the original `chtMultiRegionFoam` (solver for steady or transient fluid flow, solid heat conduction, conjugate heat transfer, buoyancy effects, turbulence, reactions and radiation modeling) plus the capability to simulate hydrogen transport in coupled fluid–solid domains, under any permeation regime and in the presence

* Corresponding author.
E-mail address: federico.hattab@uniroma1.it (F. Hattab).

https://doi.org/10.1016/j.fusengdes.2024.114362
Received 14 December 2023; Received in revised form 13 March 2024; Accepted 13 March 2024
Available online 21 March 2024

of traps. The solver is designed to perform detailed analysis of tritium-relevant components for a liquid breeder concept and will be applied to an ARC-like fusion reactor.

2. Tritium transport model description

2.1. Physical model

In a liquid immersion BB, tritium is generated inside the BB, which transports the isotope along its path, where it might interact with surrounding structures. This can be modeled as the transport of the tritium concentration C [$\mathrm{mol\,m^{-3}}$], a scalar quantity:

$$\frac{\partial C}{\partial t} + \nabla \cdot (\boldsymbol{U} C) - \nabla \cdot (D \nabla C) = S_c - \sum_{i=1}^{j} \frac{\partial C_{t\,i}}{\partial t} \tag{1}$$

$$\frac{\partial C_{t\,i}}{\partial t} = \frac{\alpha_t}{N} C (n_t - C_{t\,i}) - \alpha_d C_{t\,i} \tag{2}$$

where D [$\mathrm{m^2\,s^{-1}}$] is the diffusion coefficient, **U** [$\mathrm{m\,s^{-1}}$] is the velocity of the fluid and S_c [$\mathrm{mol\,m^{-3}\,s^{-1}}$] is a volumetric source term. Due to a hydrogen partial pressure gradient between the bulk of the fluid and surrounding structures, permeation into structural materials occurs. Inside metals, hydrogen isotopes can be trapped in so called trapping sites, leading to the presence of the sink (trapping)/source (detrapping) term in Eq. (1). Always in Eq. (1), the summation of the trapping term is over all the active traps, while Eq. (2) is the conservation equation for the trapped species $C_{t\,i}$. The trapping and detrapping rate coefficients are, respectively, α_t [$\mathrm{s^{-1}}$] and α_d [$\mathrm{s^{-1}}$], and N [$\mathrm{m^{-3}}$] is the number density of the host material. Concentrations in Eq. (1) and Eq. (2) are atomic volumetric concentrations [$\mathrm{m^{-3}}$], while n_t [$\mathrm{m^{-3}}$] is the trap density, which is computed as the product between the trap fraction f_t and N. The difference between n_t and C_t represents the number of empty trapping sites.

2.1.1. Membrane permeation

The dynamics of permeation are governed by surface (dissociation, recombination) and bulk phenomena (diffusion, trapping). If hydrogen is permeating through a metal membrane of thickness L, the molecular flux impinging onto the metal surface is given by the net flux [$\mathrm{mol\,m^{-2}\,s^{-1}}$] between the absorption flux and the desorption flux [22], as shown in Eq. (3), where subscripts f and s stand for fluid and solid:

$$J = K_d\, p_f - K_r\, C_{s,s}^2 \tag{3}$$

K_d [$\mathrm{mol\,m^{-2}\,Pa^{-1}\,s^{-1}}$] and K_r [$\mathrm{m^4\,s^{-1}\,mol^{-1}}$] are the dissociation and the recombination rate, respectively, p_f [Pa] is the hydrogen partial pressure in the fluid and $C_{s,s}$ is the concentration at the surface on the solid side. A similar equation can be written on the other side of the membrane, keeping in mind that surface properties, thus K_d and K_r, might differ on the two sides (asymmetric membrane).

At steady state, the flux in Eq. (3) on either side of the membrane is equal to the diffusion flux into the material:

$$K_d\, p_f - K_r\, C_{s,s}^2 = D \nabla C_s \tag{4}$$

Under the assumption of equilibrium (which is usually made, regardless if equilibrium is actually achieved) [14,23] K_d, K_r and the solubility K_s [$\mathrm{mol\,m^{-3}\,Pa^{-0.5}}$] are linked together through Eq. (5), while Eq. (6) determines the relationship between the hydrogen partial pressure inside the metal and its concentration:

$$K_d = K_s^2\, K_r \tag{5}$$

$$C = K_s \sqrt{p} \tag{6}$$

Depending on the material, typically in fluids, Eq. (6) might not hold and concentration and partial pressure might follow Henry's law. This happens for instance in FLiBe [24]:

$$C = K_s\, p \tag{7}$$

In (7) the solubility has units of [$\mathrm{mol\,m^{-3}\,Pa^{-1}}$].

2.1.2. Permeation regimes

When defects do not play a major role, the permeation of hydrogen presents two limiting regimes: the Diffusion Limited Regime (DLR) and the Surface Limited Regime (SLR). Let us consider the permeation factor $W = K_r\, K_s\, p^{0.5} L / D$ [22], which represents the relative rate of diffusion and surface processes. If $W \gg 1$ we are in a DLR, surface processes are much faster than diffusion processes and permeation can be modeled as a function of the latter, neglecting surface dynamics. In this case, at the interface between a fluid and a solid, one can write the continuity of partial pressures (Eq. (8)) and the conservation of hydrogen fluxes at the interface (Eq. (9)).

$$D_f \nabla C_f = D_s \nabla C_s \tag{8}$$

$$\frac{C_f}{K_{s,f}} = \left(\frac{C_s}{K_{s,s}} \right)^2 \tag{9}$$

Inside the solver the concentration gradients in Eq. (4) and in Eq. (9) are computed as the difference between the surface value and the cell center value of the field interface cells divided by the distance between the two points.

If $W \ll 1$ permeation is surface-limited and surface processes are much slower than diffusion processes, determining the dynamics of permeation. Analytical solutions for this regime have been derived by [25,26]. All transport properties are modeled as time-varying, temperature-dependent scalar fields and are modeled according to the Arrhenius equation, using a pre-exponential factor and a characteristic energy. For instance, the diffusion coefficient is defined as:

$$D = D(T) = D_0 \exp\left(\frac{-E_a}{RT} \right) \tag{10}$$

where D_0 [$\mathrm{m^2\,s^{-1}}$] is the pre-exponential factor, E_a [$\mathrm{J\,mol^{-1}}$] is the activation energy, R = 8.314 $\mathrm{J\,mol^{-1}\,K^{-1}}$ is the ideal gas constant and T [K] is the temperature.

2.2. Implementation of numerical model

The `pastaFoam` solver is based on the `chtMultiRegionFoam` solver available in OF 9 [27], which can simulate transient, buoyant, turbulent fluid flow and solid heat conduction, along with conjugate heat transfer between fluid and solid regions. The solution strategy followed by the solver is segregated: first, all the fluid regions are solved, solving sequentially the field equations, then solid regions are solved using the solution of the fluid regions as Boundary Condition (BC) at the fluid–solid interfaces. The accuracy on regions coupling may be increased performing several `PIMPLE` loops, which is the pressure–velocity coupling algorithm adopted [28]. Concerns regarding errors in the mass conservation of tritium when coupling two regions under this solution strategy have been raised by [14], but such discrepancies have not been encountered in this work, possibly due to the different implementation of the coupling BC.

To couple fluid and solid regions two BCs have been developed, both derived from the existing `turbulentTemperatureCoupledBaffleMixed` BC used to perform temperature coupling. The original BC imposes a system of two equation consisting of the continuity of temperatures and the conservation of heat fluxes at the interface, using an OF mixed BC:

$$T_{wall} = valueFr \cdot \omega + (T_{cellcenter} + \Delta \cdot refGrad)(1 - \omega) \tag{11}$$

where Δ is the inverse of the distance between the cell center and the cell surface. One can derive the values for valueFr, ω and refGrad by solving for the system of two equations.

For the DLR, the `DLRTritiumCoupledMixed` BC has been developed in complete analogy with the original implementation for temperature, imposing Eq. (8) and Eq. (9). For the more general formulation that considers surface effects, the `tritiumCoupledMixed` BC has been developed imposing Eq. (7) and Eq. (4). The main feature for both

Table 1
Relative errors and integral errors for the verification cases presented in this work.

Case ref.	Fig. ref.	RE (%)	IE (%)	Data compared to
Section 3.1.1	Fig. 1(a)	0.02	0.02	analytical
Section 3.1.1	Fig. 1(b)	0.49	0.23	analytical
Section 3.1.2	Fig. 2	0.00	0.00	analytical
Section 3.1.3	Fig. 3	0.15	–	analytical
Section 3.1.3	Fig. 4	1.40	–	analytical
Section 3.1.4	Fig. 4(a)	0.29	0.07	analytical
Section 3.1.4	Fig. 4(b)	0.17	0.05	analytical
Section 3.2	Fig. 6	0.004	0.004	analytical
Section 3.2	Fig. 7	0.62	0.62	analytical
Section 3.3.1	Fig. 8	0.007	0.004	analytical
Section 3.3.2	Fig. 9	–	0.2	code-to-code with Ref. [14]
Section 3.3.3	Fig. 10	–	0.08	code-to-code with Ref. [14]
Section 3.4.1	Fig. 11	72.0	–	exp. [29]
Section 3.4.1	Fig. 12	20.3	–	exp. [30]
Section 3.4.2	Fig. 13	022.8	0.4	exp. [31]

formulations is that the quadratic term in the resulting equation has been decomposed in two terms, leveraging the iterative numerical resolution approach intrinsic to the code, to maintain the same linear formalism used for temperature.

The concentrations have been added as volumetric scalar fields and the solver solves for them using Eq. (1) and Eq. (2), respectively (minus the advective term in the transport equation for solids). Traps are present only in solid regions and, at the moment, one single trap is modeled, but the extension to multiple traps is straightforward.

3. Model verification & validation

In this chapter a series of verification and validation cases are presented. Comparisons with TMAP8, the solver developed by [14] and with TRIDENT [11] are made. Where indicated, Integral Errors (IE) are computed according to Eq. (12) as the complement to one of the ratio of the numerical and the reference areas delimited by the n data points.

$$IE = 100\left|\frac{\sum_{i=1}^{n} A_{OF\,i,i+1}}{\sum_{i=1}^{n} A_{ref\,i,i+1}} - 1\right| \tag{12}$$

$$RE = \frac{100}{n}\sum_{i=1}^{n}\left|\frac{value_{OF,i}}{value_{ref,i}} - 1\right| \tag{13}$$

Relative Errors (RE) are instead computed as the complement to one of the ratio of the numerical and the reference values. For all cases hexahedral, structured and coherent meshes have been used, with grading towards boundaries in the direction of the permeation flux when needed. The discretization schemes adopted are of the second order for both temporal and spatial discretization.

A summary of the results obtained in the verification and validation cases shown in this work is reported in Table 1.

3.1. Analytical cases

3.1.1. Diffusion in a slab with constant source BC

In this verification case taken from [9], the ability of the solver to reproduce a simple diffusion problem is tested. Permeation through a 200 m long slab of SiC is modeled, considering a constant source C_0 equal to one on the left boundary of the slab. The initial concentration is zero and diffusivity is taken as unity. The analytical solution for the concentration is given by [32], where t [s] is the time and x [m] is the distance from the left boundary:

$$C = C_0 erfc\left(\frac{x}{2\sqrt{D\,t}}\right) \tag{14}$$

Results are shown in Fig. 1. The IE and RE with respect to the analytical solution for Fig. 1(a) are both 0.02% and are the same as TMAP8, while for Fig. 1(b) the IE is 0.2%, higher than the 0.1% of TMAP8 and the RE is 0.5%, lower than the 1.5% in TMAP8 (Table 1).

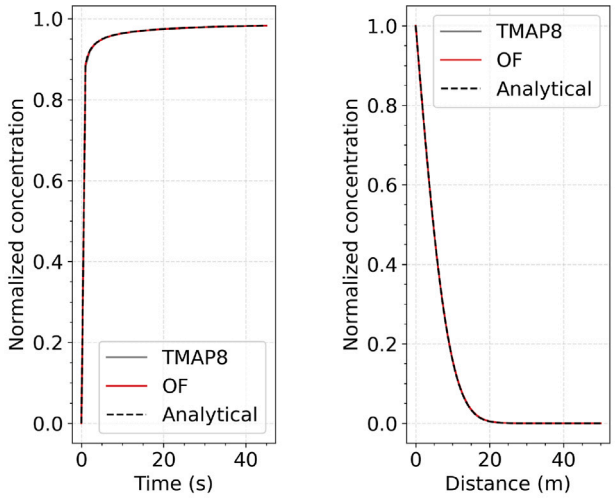

(a) Normalized concentration over time 2 mm into the slab. **(b)** Normalized concentration into the slab after 25 seconds.

Fig. 1. Diffusion in a semi-infinite slab with constant source BC.

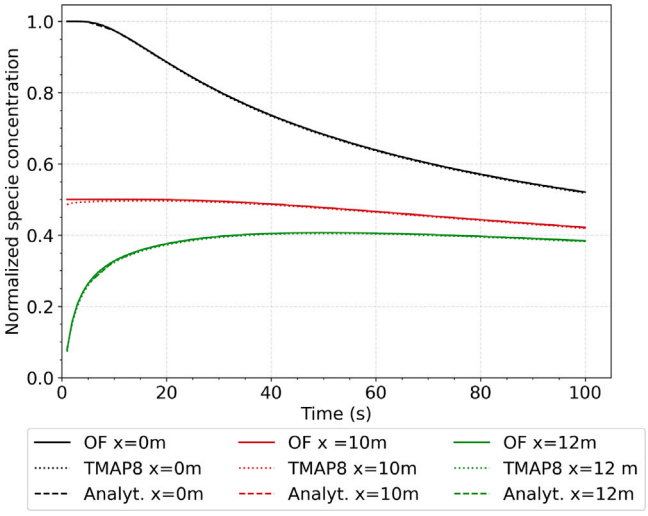

Fig. 2. Concentration vs time for the diffusion in a semi-infinite slab preloaded with an initial concentration C_0 in the first 10 m. Plots are shown for x = 0, 10 and 12 m.

3.1.2. Diffusion in a partially preloaded slab

Permeation into a 100 m long slab of SiC is analyzed, considering that the first 10 m of the slab are preloaded with an initial concentration C_0, while the rest of the slab is initialized at C = 0. D and C_0 are taken as unity. The simulation time is 100 s. Both the `pastaFoam` and TMAP meshes are made of 1000 elements along the length of the slab. This case tests the behavior of the solver under nonuniform initial conditions. In Fig. 2 the evolution of the concentration over time is shown, at the inlet of the slab and 10 and 12 meters away from the inlet. The case is taken from [9] and the analytical solution for the concentration is given by [32]:

$$C = \frac{C_0}{2}\left[erf\left(\sqrt{D\,t}\frac{h-x}{2}\right) + erf\left(\frac{h+x}{2\sqrt{D\,t}}\right)\right] \tag{15}$$

Agreement of `pastaFoam` with the analytical solution is excellent (IE and RE less than 0.001%, Table 1).

3.1.3. Permeation through a membrane with trapping

This case from [9] tests the trapping functionality of the solver. Permeation through a 1 m thick membrane at 1000 K with active

traps is simulated. The region is initially empty. On the inlet side a `fixedValue` BC is used to set a constant atomic source of 3.1622×10^{18} m^{-3} for C, while the outlet side concentration is kept at zero. The solver is coded to accept molar concentrations, but when trapping is turned on all input molar quantities must be converted to atomic ones. D is taken as unity, while the trapping rate α_t is set constant and equal to 1×10^{15} s^{-1}. The detrapping rate α_d is defined as:

$$\alpha_d = 1\times10^{13}\cdot\exp\left(-\frac{\epsilon/k}{T}\right) \tag{16}$$

where ϵ is the trap energy and k is Boltzmann's constant. To evaluate numerical results a comparison between the analytical and the numerical breakthrough time is made. Depending on the trapping regime, the breakthrough time can have two different limiting values. The trapping regime can be determined by comparing the trapping parameter ζ defined in Eq. (17) with the ratio between the mobile concentration and the trap fraction C/f_t. $\lambda = 3.162\times10^{-8}$ m is the lattice parameter, $\nu = 1\times10^{13}$ s^{-1} is the Debye frequency, $D_0 = 1$ m^2 s^{-1} is the pre-exponential factor of the Arrhenius equation for diffusivity and E_d is the diffusion activation energy. For f_t a value of 0.1 is considered.

$$\zeta = \frac{\lambda^2\nu}{D_0\,\rho}\exp\left(\frac{E_d-\epsilon}{kT}\right)+\frac{C}{f_t} \tag{17}$$

If $\zeta \gg C/f_t$, then diffusion is the rate-limiting process and the effective diffusivity regime applies. The transient is similar to the standard diffusion but an effective diffusivity D_{eff} (Eq. (18)) must be considered. In this case, the analytical solution for the transient permeation flux is give by [10]:

$$D_{eff} = \frac{D}{1+\sum_j \frac{1}{\zeta_j}} \tag{18}$$

$$J = \frac{C_0 D}{L}\left\{1+2\sum_{i=1}^{\infty}\left[(-1)^i\exp\left(-m^2\frac{L}{\tau_{bc}}\right)\right]\right\} \tag{19}$$

$$\tau_{bc} = \frac{L^2}{2\pi^2 D_{eff}} \tag{20}$$

where L is the thickness of the slab and τ_{bc} is the breakthrough time, defined as the intersection of the steepest tangent to the diffusion flux plot over time with the time axis (Eq. (20) and Eq. (18)).

If $\zeta \approx C/f_t$ then, the trapping is the rate-limiting process and the strong trapping regime applies. In this case, there is little to no permeation until the traps are filled and then the flux quickly reaches its steady state value. Here, the breakthrough time can be defined as the time it takes for the flux to reach 99% of its steady state value and is given in formula by:

$$\tau_{bd} = \frac{L^2 f_t}{2C_0 D} \tag{21}$$

Results for the effective diffusivity regime are shown in Fig. 3. `pastaFoam` and TMAP8 perform very similarly with respect to the analytical solution, with an error of 0.15% on the breakthrough time (Table 1).

Results for the deep trapping regime are shown in Fig. 4. The breakthrough time obtained in `pastaFoam` and TMAP8 are 507 and 477 s, while the analytical one is 500 s (RE with respect to the analytical of 1.38% and 4.6%, respectively, Table 1).

3.1.4. Diffusion in composite membrane

This verification case is taken from [10] and tests the `DLRTritiumCoupledMixed` BC. The computational domain is composed of two regions, a PyC layer 33 μm thick followed by a Sic layer 66 μm thick. The same nodalization of 1000 uniform elements used in TMAP8 along the thickness of the membrane was used in pastaFoam. On the left boundary of the PyC region the inlet concentration is fixed to $C_0 = 50.7079$ mol m−3, while on the right boundary of the SiC region a zero concentration BC is used. Diffusivity values are taken as constants and equal to 1.274×10^{-7} m^2 s^{-1} for the PyC and 2.622×10^{-11} m^2 s^{-1} for SiC. Solubility is taken as unity for both materials. Analytical transient solutions for the two materials can be found in [10] and numerical results obtained with OF are shown in Fig. 5. `pastaFoam` IE is 0.07% and 0.05% for Figs. 4(a) and 4(b) (Table 1), respectively, and are similar to the errors with TMAP8 (0.1% and 0.01%).

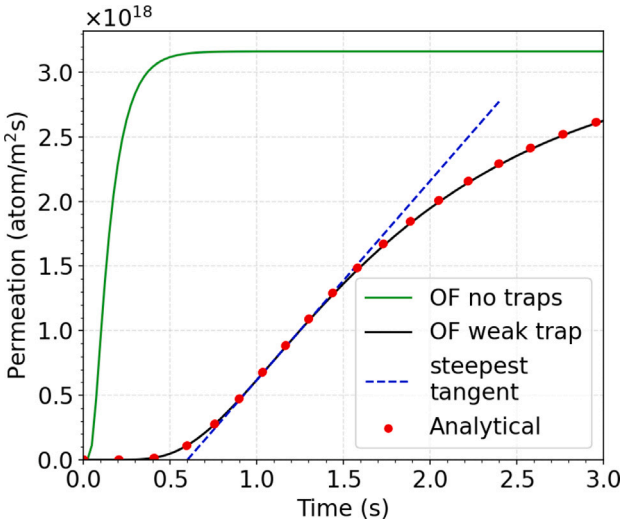

Fig. 3. Atomic flux vs time for the diffusion in a slab with active trap under effective diffusivity regime.

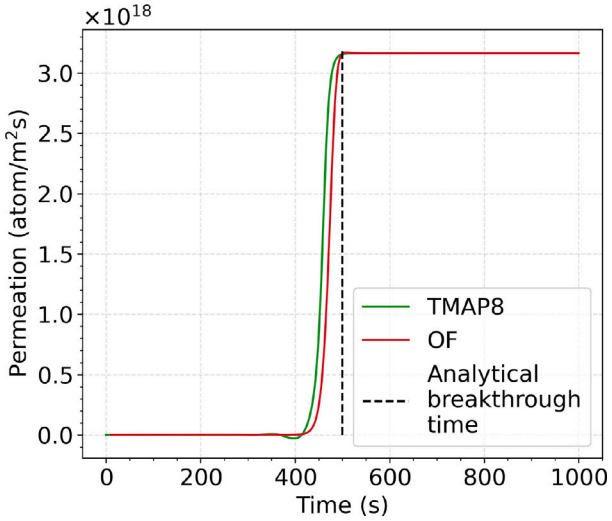

Fig. 4. Atomic flux vs time for the diffusion in a slab with active trap under strong trapping regime.

3.2. SLR analytical solution

In this section the `tritiumCoupledMixed` BC is tested under SLR. A gas-driven permeation of hydrogen through a 1 mm thick membrane is studied. The membrane is in contact with an upstream fluid volume kept at a constant pressure $p = 4\times10^{-4}$ Pa and a downstream fluid volume constantly evacuated from the permeated gas. The analytical solution to the problem is taken from [25,26], which provide an equation for the time evolution of the flux J and the concentration C during surface-limited permeation through a membrane:

$$J = J_m\frac{\left[\tanh(t/\tau)+C_0/C_m\right]^2}{\left[(C_0/C_m)\times\tanh(t/\tau)+1\right]^2} \tag{22}$$

$$C = C_m\times\tanh^2\left[t/\tau+\operatorname{arctanh}(C/C_0)\right] \tag{23}$$

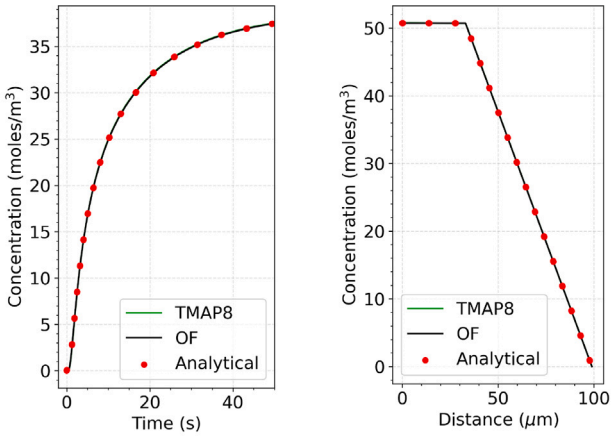

(a) Concentration into the SiC layer vs time 48.75 μm away from the PyC left boundary.

(b) Concentration vs distance at steady state over the whole domain.

Fig. 5. Diffusion in a composite membrane.

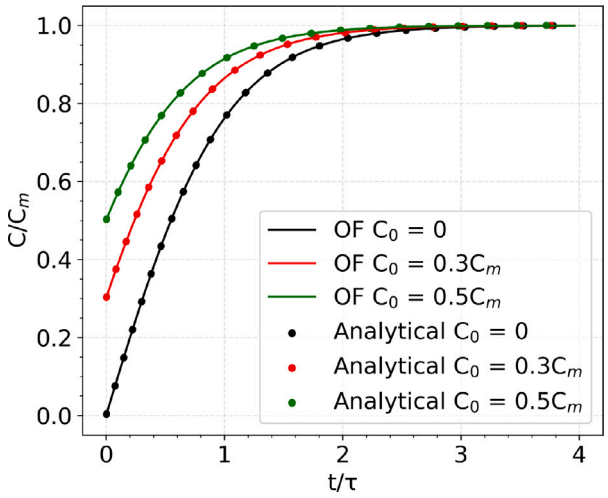

Fig. 6. Normalized concentration as a function of time for three different initial values in the membrane.

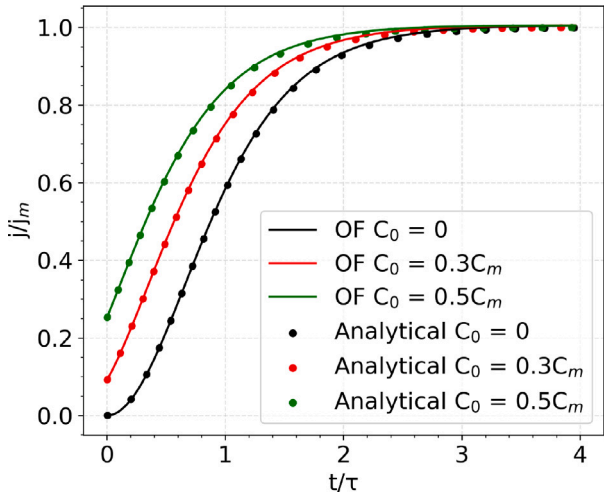

Fig. 7. Normalized permeation flux as a function of time for three different initial concentration in the membrane.

$$J_m = K_s^2\, p K_{r1} K_{r2} (K_{r1} + K_{r2})^{-1} \tag{24}$$

$$C_m = K_s\, p^{1/2} K_{r1}^{1/2} (K_{r1} + K_{r2})^{-1/2} \tag{25}$$

$$\tau = L\, K_s^{-1}\, p^{-1/2} \left[K_{r1}(K_{r1} + K_{r2})\right]^{-1/2} \tag{26}$$

where J_m and C_m are the steady state flux and concentration, respectively, L is the membrane thickness and τ is the characteristic time, defined as the time it takes for the concentration to reach its steady state value if the initial concentration is zero and there is no release from the membrane. The subscripts 1 and 2 indicate the left and right side of the membrane.

The different treatment of the two surfaces is because the analytical model, as well as the solver, can take into account asymmetries in the membrane, thus different values of K_r and K_d for a single region can be considered. The parameters used for the analysis are: D= 1 $m^2\,s^{-1}$, K_s= 1×10^{27} mol m^{-3} Pa^{-1}, $K_{r1} = K_{r2} = 1 \times 10^{-30}$ $m^4\,s^{-1}$ mol^{-1} and$T$ = 773 K. With this setup the permeation parameter W is $\ll 1$ and SLR is ensured.

Inside the `pastaFoam` computational domain two fluid regions with a solid one in the middle have been considered. They are coupled together using the `tritiumCoupledMixed` BC for concentration, while on the left boundary of the upstream region and on the right boundary of the downstream region concentration is fixed to $p \times K_s$ and zero, respectively. The fluid regions are 0.1 mm thick and all regions meshes have grading towards coupled boundaries. Results for three different initial concentrations are shown in Fig. 6 and in Fig. 7. Agreement for the concentration is excellent (IE and RE < 0.004%) and the error (IE and RE) for the flux, computed in post-processing, is 0.62% (Table 1).

3.3. Benchmark with existing openfoam tritium migration models

To address concerns raised by [14] and verify the equivalence of the modeling with the present work, in this section three cases reported in [14] are reproduced. The benchmark is limited to the functionalities used in the reference cases, that is, the transport equation and the coupling under diffusion limited regime.

3.3.1. Diffusion in a membrane with constant BCs

This case is analogous the one in Section 3.1.1 and is take from [33], which describes the analytical solution in Section 4.3.3. Hydrogen permeates through a 1.2 mm thick membrane fixing the concentration at the left (1) and right (2) boundary of the domain. The initial concentration C_0 is equal to the right boundary fixed value C_2 and is equal to 8.3×10^{-15} mol m^{-3}, while on the left side we have C_1 = 0.83 mol m^{-3}. D is constant and equal to $1.119\,018 \times 10^{-8}$ $m^2\,s^{-1}$. The mesh is the same as the reference case, $90 \times 2 \times 2$ elements, and the timestep is 5 ms. The transient evolution of the concentration profile is shown in Fig. 8. Agreement with the analytical solution is excellent (less than 0.01% both for RE and IE at 30 s into the simulation, Table 1).

3.3.2. Transient gas-driven permeation

This case reproduces the permeation of deuterium through a membrane separating two volumes. The upstream volume is kept at a partial pressure of 10 Pa, while the downstream one has an initial concentration of 0 Pa and is assumed to be closed. The analytical formula for the pressure evolution in the downstream volume is derived from [33], formula (4).24a, page 51. Modeling parameters and choices are the same as [14]. The membrane is assumed to be made of 9%-Cr RAFM steel and transport data for Deuterium are taken from [34]. The computational domain is made of three regions, coupled with each other with the `DLRTritiumCoupledMixed` BC. The yz cross-section of the entire mesh is made of 4 cells, while along the x axis the upstream fluid region, the membrane and the downstream fluid region are made

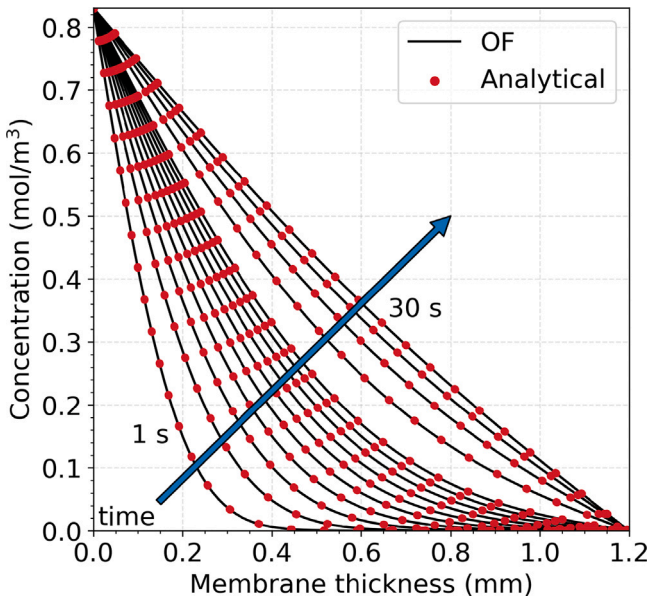

Fig. 8. Diffusion in a membrane with constant BCs. Concentration profile over the thickness of the membrane at different times, from 1 s to 30 s.

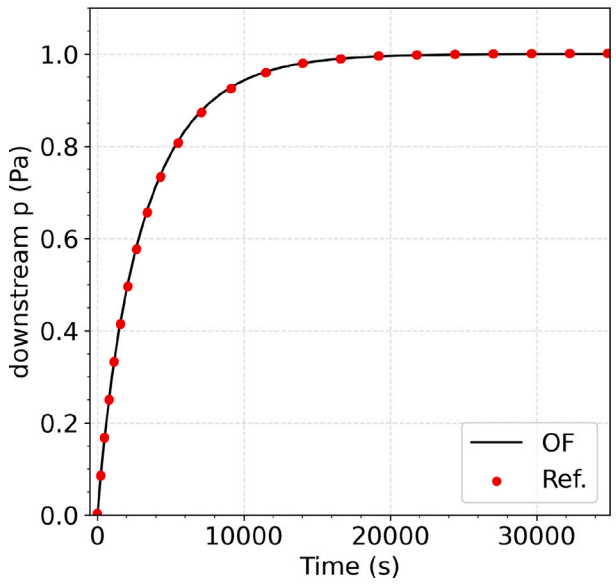

Fig. 10. Transient H gas driven permeation through a Eurofer-97 membrane. This work (OF) vs Ref. [14]. Pressure evolution in the downstream fluid volume.

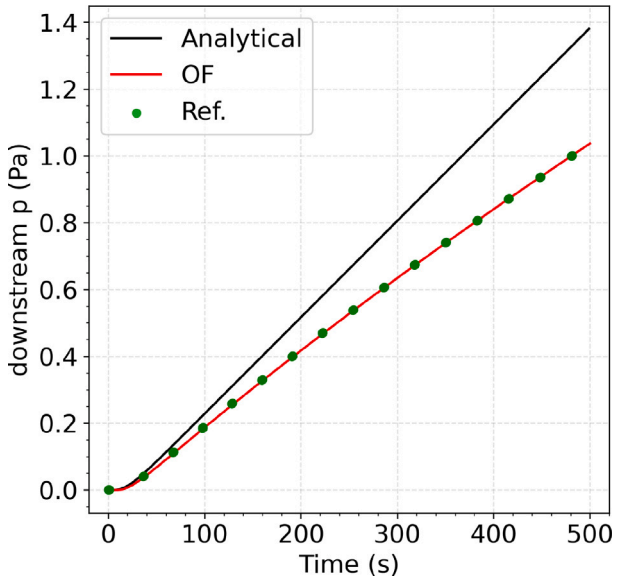

Fig. 9. Permeation of Deuterium through a 9%-Cr RAFM steel membrane. OF (pastaFoam) is this work, Ref. is [14]. Analytical formulation does not consider pressure buildup in the downstream volume.

of 10, 100 and 1 cell, respectively. To avoid the influence of gas diffusion in the fluid regions, a diffusivity of 1 was considered for both volumes. Results are shown in Fig. 9. Agreement with [14] is excellent (IE ~0.2%, Table 1) and the deviation from the analytical solution is due to the fact that pastaFoam takes into account the pressure buildup in the downstream volume, while this is not considered in the analytical formulation, which assumes the downstream pressure to be zero.

3.3.3. Transient gas-driven permeation 2

This case is very similar the one presented in Section 3.3.2 and was meant to be a comparison with the TMAP7 code. Two volumes of 1×10^{-3} m^3 and with initial hydrogen partial pressure of 1×10^{-3} Pa are separated by a 1.2 mm thick Eurofer-97 membrane. Temperature is uniform and equal to 723 K. Pressure in the upstream volume is ramped up from the initial value to 1 Pa during the first second of simulation and it is then kept constant. The membrane is made of 10 cells in the x direction and the two neighboring volumes present grading towards the interface with the membrane. Concentration is fixed at the left boundary of the upstream volume to obtain the desired input pressure, the fluid-membrane interfaces utilize the `DLRTritiumCoupledMixed` BC and all other boundaries are set up with a `zeroGradient` BC. Fig. 10 shows the pressure evolution in the downstream volume and agreement of the pressure trend with the reference case is close to perfect (IE ~0.08%, Table 1).

3.4. Experimental cases

3.4.1. Permeation experiments in flinak & flibe

Considering the application of `pastaFoam` to ARC-like reactors, testing on experiments with molten salts is of great interest. In the absence of data for forced-convection molten salt system containing tritium or other hydrogen isotopes, two static permeation experiments, one using FLiNaK [29] and one using FLiBe [30] have been considered. Both experiments were done on the same experimental apparatus described in [29] and a schematic diagram of it can be seen in Fig. 1 of [29]. The aim of the experiments was to measure permeability, solubility and diffusivity of hydrogen in FLiNaK [29] and diffusivity and solubility of tritium in FLiBe [30]. A mixture of H_2/T_2 and argon (Ar) is introduced into the bottom of the test section at a constant flow rate and pressure. This mixture is in contact with the test section, which has a 2 mm thick Ni lower plate and contains a known volume of static FLiNaK/FLiBe. Permeation of atomic hydrogen through the Ni plate followed by recombination and diffusion through the molten-salt layer takes place. An Ar purge flow removes permeated hydrogen from the salt free surface. Parameters used in `pastaFoam` to reproduce the two experimental campaigns are shown in Table 2 and in Table 3. Upstream pressures and experimental data have been extracted from Fig. 3 in [29] and from Fig. 2 in [30].

The numerical model is made of a solid and a fluid region stacked on top of each other. Concentration at the base of the nickel plate and at the top of the fluid region is fixed, the interface is modeled with the `tritiumCoupledMixed` BC and all other boundaries are modeled as `zeroGradient`. The Nickel plate is modeled with 5 elements along the thickness of the plate, the FLiNaK with 50 elements and the FLiBe

Table 2
Input parameters for pastaFoam simulation of the experimental campaign presented in [29].

Parameter	Value–Range
H_2 input pressure [Pa]	1×10^5–1×10^3
H_2 cover gas pressure [Pa]	0
Temperature [K]	773, 873, 973
FLiNaK thickness [mm]	20
Ni membrane thickness [mm]	2
D_{FLiNaK} [$m^2\ s^{-1}$]	$0.38–1.9 \times 10^{-8}$ Ref. [29]
$K_{s\,FLiNaK}$ [$mol\ m^{-3}\ Pa^{-1}$]	$8.4–2.8 \times 10^{-5}$ Ref. [29]
D_{Ni} [$m^2\ s^{-1}$]	$1.5–5.3 \times 10^{-9}$ Ref. [35]
$K_{s\,Ni}$ [$mol\ m^{-3}\ Pa^{-0.5}$]	$4.8–8.0 \times 10^{-2}$ Ref. [35]
$K_{d\,Ni}$ [$mol\ m^{-2}\ s^{-1}\ Pa^{-1}$]	$1.4–3.7 \times 10^{-8}$ Ref. [36]

Table 3
Input parameters for pastaFoam simulation of the experimental campaign presented in [30].

Parameter	Value–Range
H_2 input pressure [Pa]	1210–171
H_2 cover gas pressure [Pa]	0
Temperature [K]	823, 873, 923, 973
FLiBe thickness [mm]	81
Ni membrane thickness [mm]	2
D_{FLibe} [$m^2\ s^{-1}$]	$2.0–5.2 \times 10^{-9}$ Ref. [30]
$K_{s\,FLiBe}$ [$mol\ m^{-3}\ Pa^{-1}$]	$0.47–1.0 \times 10^{-3}$ Ref. [30]
D_{Ni} [$m^2\ s^{-1}$]	$1.3–3.1 \times 10^{-9}$ Ref. [35]
$K_{s\,Ni}$ [$mol\ m^{-3}\ Pa^{-0.5}$]	$5.6–8.0 \times 10^{-2}$ Ref. [35]
$K_{d\,Ni}$ [$mol\ m^{-2}\ s^{-1}\ Pa^{-1}$]	$1.9–3.7 \times 10^{-8}$ Ref. [36]

with 200 elements. A mesh sensitivity analysis has shown independence of results from the selected mesh. Also smaller timesteps have been tested to assess its influence over steady-state values. Of the different configurations shown in Table 4 and tested on the run at 973 K and 1×10^5 Pa, no significant variation in flux at steady state is observed with respect to the coarser mesh analyzed. Steady state permeation fluxes at different temperatures and pressures are shown in Fig. 11 (experiment from [29]) and Fig. 12 (experiment from [30]). The average error on the experimental campaign from [29] is 72%, which goes down to 42.5% if only the single data point at 10^4 Pa and 773 K is neglected. Significant differences in flux have been observed changing the transport properties for hydrogen in nickel, and this is considered the biggest source of uncertainty for these cases. The average error on the experimental campaign from [30] is 20.3% (Table 1). The same cases have been simulated in the TRIDENT code by [23], and extracting data from Fig. 5.23 (runs with FLiNaK) and Fig. 5.24 (runs with FLiBe) in [23], average errors of 102.8% and 34.3% were found, respectively. As argued by [23], one source of deviation for computed value with respect to experimental results in [30] might be due to the fact that in TRIDENT, as well as in pastaFoam, the assumption that all tritium exists as T_2 is made, however the measured $K_{s\,flibe}$ in [30] matches more closely the value for tritium fluoride rather than that for T_2. This highlights the importance of chemistry control of the salt when performing experiments and modeling real salt-based systems. As already mentioned above, the uncertainty in tritium transport properties for cases [29,30] can significantly impact the accuracy of reproducing experimental measurements. When validating software, to mitigate any deviation, it is important to compare results with experiments where the chemical state of all materials involved in the migration of tritium is well-known. The transport properties employed in numerical computations should accurately reflect the state of said materials during the experiment.

3.4.2. Diffusion experiment in beryllium sample

In this section the experimental data presented by [31] in Fig. 2 (a) is simulated in pastaFoam. In the paper, deuterium ion implantation, thermal absorption and desorption experiments on thin layers of high-purity beryllium were conducted. The experiment of interest

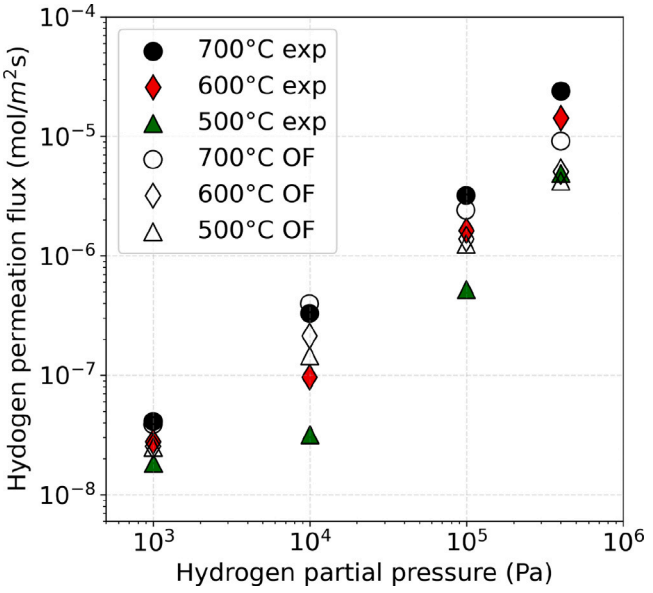

Fig. 11. Steady state H_2 permeation flux through Ni and FLiNaK at different temperatures and input pressures. This work (OF) vs Ref. [29] (exp). Permeation is gas-driven and the molten salt is static.

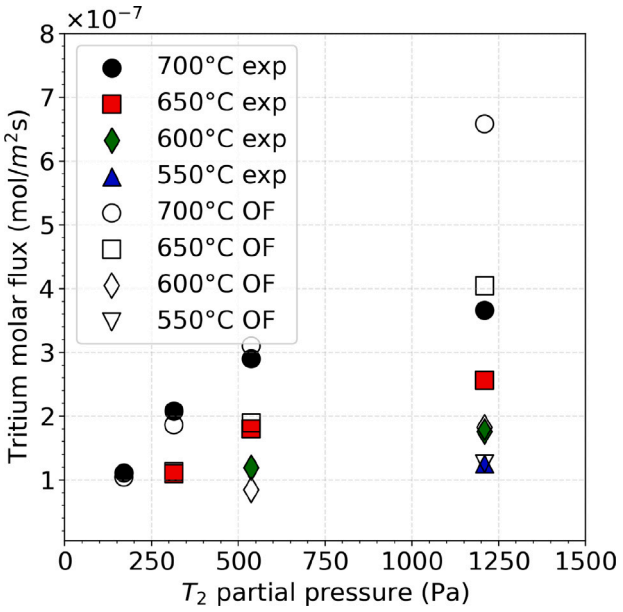

Fig. 12. Steady state T_2 permeation flux through Ni and FLiBe at different temperatures and input pressures. This work (OF) vs Ref. [30] (exp). Permeation is gas-driven and the molten salt is static.

Table 4
Mesh and timestep sensitivity analysis on experimental run from [29] at 973 K and 1×10^5 Pa. E% is with respect to the reference model "Ref".

Run ID	Mesh Ni	Mesh FLiNaK	Grading	dt (s)
Ref	3 × 5 × 1	3 × 50 × 1	no	1
m1	3 × 10 × 1	3 × 100 × 1	no	1
m2	3 × 20 × 1	3 × 200 × 1	no	1
m3	3 × 20 × 1	3 × 200 × 1	yes	1
m4	3 × 40 × 1	3 × 400 × 1	no	1
t1	3 × 5 × 1	3 × 50 × 1	no	0.1
t2	3 × 5 × 1	3 × 50 × 1	no	0.01

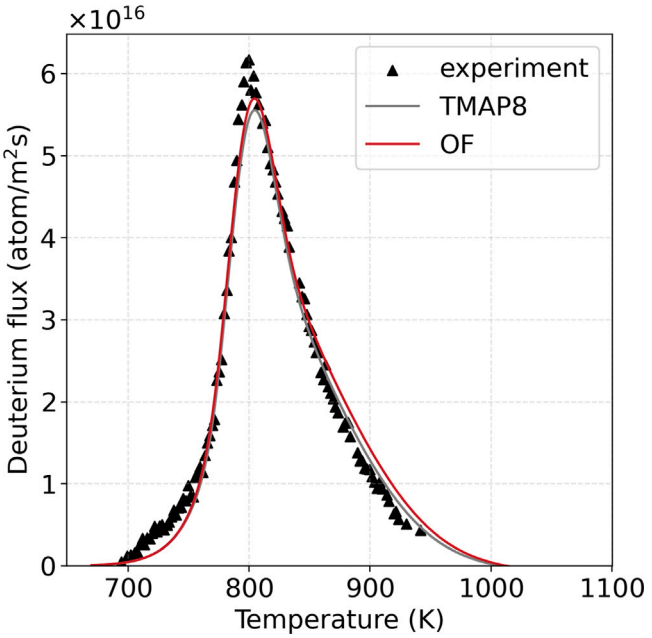

Fig. 13. Deuterium flux through beryllium sample during a thermal desorption test. Experimental points are from Fig. 2 (a) in [31].

Table 5
Meshe discretizations considered in the mesh sensitivity analysis on experimental data from [31]. The beryllium region is modeled with two boxes, of which the first has the same dimensions and discretization of the BeO region.

Run ID	Mesh BeO	Mesh Be	
	box1	box1	box2
m1	2 × 3 × 1	2 × 3 × 1	235 × 3 × 1, grading = 700
m2	3 × 3 × 1	3 × 3 × 1	354 × 3 × 1, grading = 700
m3	6 × 3 × 1	6 × 3 × 1	710 × 3 × 1, grading = 700
Ref	8 × 3 × 1	8 × 3 × 1	947 × 3 × 1, grading = 700
m5	10 × 3 × 1	10 × 3 × 1	1184 × 3 × 1, grading = 700

was conducted on a 0.4 mm thick sample of pure, polished beryllium. On the surface of the sample a 18 nm beryllium oxide (BeO) film was measured via Rutherford backscattering measurements. The sample was first positioned in a charging furnace and exposed to deuterium at 13.3 kPa and 773 K for 50 h. Then it was cooled under a vacuum of 1×10^{-6} Pa with a time constant of 45 min. Once cooled down to 300 K, the sample was transferred to a thermal desorption furnace where it was heated under a vacuum of 1×10^{-3} Pa up to 1073 K. The furnace heating rate was 3 K/min. This experiment was reproduced in TMAP8, modeling half of the sample with a reflective BC at the mid-plane of the domain. The model is made of two-segments, the first with 36 elements representing the BeO and the second with 40 elements representing pure beryllium. Also in `pastaFoam` half of the domain was simulated, using a symmetry BC at the mid-plane. The model is made of two solid regions coupled together by the `DLRTritiumCoupledMixed` BC. The BeO film is modeled with 8 uniform elements across its thickness, while the beryllium region is made of 8 elements equal to those of the Beo close to the coupled interface, followed by 947 elements that increase gradually in length, with a cell-to-cell expansion ratio of 1.007. A mesh sensitivity analysis (Table 5), of which results are shown in Fig. 14, highlights that further refining of the mesh does not lead a change in computed flux. Deuterium transport data in beryllium and in BeO are the same used by [10].

Fig. 13 shows the permeation flux of deuterium during the thermal desorption phase. Experimental points are taken from Fig. 2(a) in [31]. Integral errors for `pastaFoam` and TMAP8 are 0.4% and 4.3%, respectively (Table 1). While `pastaFoam` gets closer to the experimental peak around 800 K, it slightly over-predicts the flux compared to TMAP

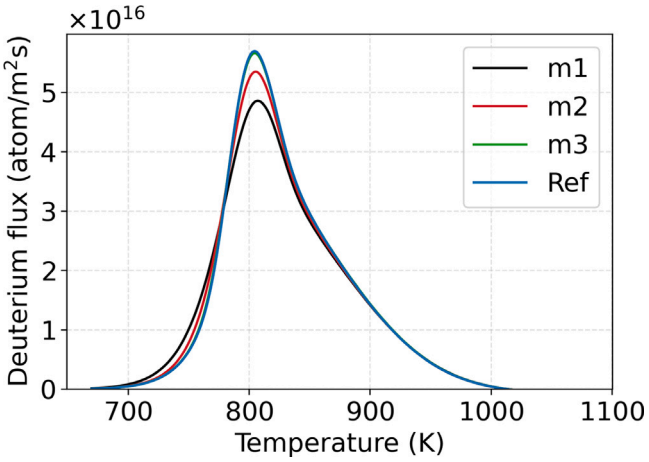

Fig. 14. Mesh sensitivity for the model developed to reproduce the case from [31]. See Table 5 for a description of the differences between the cases.

in the lower-right portion of the curve. The IE is smaller because the overall area under the curve is closer to the experimental one. On the other hand, looking at the relative error `pastaFoam` averages a 22.8% while TMAP a 20.3%. The main difference is in the left tail of the plot, where a majority of data points is clustered. Overall correlation with experimental values is excellent, with a coefficient of determination equal to 0.98 for both codes.

4. Conclusions

In this work the OpenFOAM `pastaFoam` solver for transient tritium transport was presented, along with two coupling BCs for hydrogen mass transfer. The solver can simulate tritium transport with or without traps in coupled fluid–solid systems and leverages all the capabilities of the base `chtMultiRegionFoam` solver. Coupling is done both under the assumption of DLR and accounting for surface effects. An extensive list of verification and validation cases was performed, as summarized in Table 1. Verification against analytical solutions and code-to-code comparisons show excellent results. Errors for validation cases are non-negligible, possibly due to uncertainties on experimental values of tritium transport parameters and experimental conditions, but are nonetheless in line with or better than results obtained with existing codes taken into consideration. Outstanding activities are the simulation of more complex 3D experimental campaigns, using data from these experiments as it becomes available. The solver here presented could be useful in scenarios where typical system-level codes struggle to model the physics at play due to their modeling approach. The solver could be used to evaluate the hydrogen mass transport coefficient h_m from the bulk of fluids to solid surfaces, taking into account real geometries and turbulent fluid flows. Experimental correlations for h_m are scarce or non-existent for fluid of interest in fusion reactors such as liquid metals (LiPb) and molten salts (FLiBe, FLiNaK). At the moment, the standard approach is to apply heat and mass transfer analogies on correlation developed for heat transfer in other fluids.

In the future, the capabilities of the code will bi extended considering multiple hydrogen species, chemical reactions and the development of a hydrogen implantation flux in solid structures. Furthermore, the code will be improved by also considering magnetohydrodynamic effects, fundamental for BB which used liquid metals, for which two solvers are currently being developed at NERG [37].

CRediT authorship contribution statement

Federico Hattab: Writing – original draft, Visualization, Validation, Software, Methodology, Investigation, Conceptualization. **Simone**

Siriano: Writing – review & editing, Software, Methodology, Conceptualization. **Fabio Giannetti:** Writing – review & editing, Supervision, Funding acquisition.

Declaration of competing interest

The authors declare that they have no known competing financial interests or personal relationships that could have appeared to influence the work reported in this paper.

Data availability

The authors do not have permission to share data.

Acknowledgments

Project ECS 0000024 Rome Technopole, - CUP B83C22002820006, NRP Mission 4 Component 2 Investment 1.5, Funded by the European Union - NextGenerationEU.

This work has been carried out within the framework of the EUROfusion Consortium, funded by the European Union via the Euratom Research and Training Programme (Grant Agreement No 101052200 — EUROfusion). Views and opinions expressed are however those of the author(s) only and do not necessarily reflect those of the European Union or the European Commission. Neither the European Union nor the European Commission can be held responsible for them.

References

[1] B. Sorbom, J. Ball, T. Palmer, F. Mangiarotti, J. Sierchio, P. Bonoli, C. Kasten, D. Sutherland, H. Barnard, C. Haakonsen, et al., ARC: A compact, high-field, fusion nuclear science facility and demonstration power plant with demountable magnets, Fusion Eng. Des. 100 (2015) 378–405.

[2] A. Kuang, N. Cao, A.J. Creely, C.A. Dennett, J. Hecla, B. LaBombard, R.A. Tinguely, E.A. Tolman, H. Hoffman, M. Major, et al., Conceptual design study for heat exhaust management in the ARC fusion pilot plant, Fusion Eng. Des. 137 (2018) 221–242.

[3] J.W. Bae, E. Peterson, J. Shimwell, ARC reactor neutronics multi-code validation, Nucl. Fusion 62 (6) (2022) 066016.

[4] F.A. Hernández, P. Pereslavtsev, G. Zhou, Q. Kang, S. D'Amico, H. Neuberger, L.V. Boccaccini, B. Kiss, G. Nádasi, L. Maqueda, et al., Consolidated design of the HCPB breeding blanket for the pre-conceptual design phase of the EU DEMO and harmonization with the ITER HCPB TBM program, Fusion Eng. Des. 157 (2020) 111614.

[5] Y. Song, J. Li, Y. Wan, Y. Liu, X. Wang, B. Wan, P. Fu, P. Weng, S. Wu, X. Duan, et al., Engineering design of the CFETR machine, Fusion Eng. Des. 183 (2022) 113247.

[6] J.S. Park, S. Kwon, K. Im, K. Kim, T. Brown, G. Neilson, Pre-conceptual design study on K-DEMO ceramic breeder blanket, Fusion Eng. Des. 100 (2015) 159–165.

[7] P. Arena, A. Del Nevo, F. Moro, S. Noce, R. Mozzillo, V. Imbriani, F. Giannetti, F. Edemetti, A. Froio, L. Savoldi, et al., The DEMO water-cooled lead–lithium breeding blanket: Design status at the end of the pre-conceptual design phase, Appl. Sci. 11 (24) (2021) 11592.

[8] K. Jiang, Y. Yu, X. Ma, Y. Yu, J. Yang, L. Chen, K. Huang, L. Chen, N. Zhang, M. Ni, et al., Research on the thermal hydraulic design of COOL blanket for CFETR, Fusion Eng. Des. 176 (2022) 113053.

[9] G.R. Longhurst, D. Holland, J. Jones, B. Merrill, TMAP4 Users manual, Tech. Rep., EG and G Idaho, Inc., Idaho Falls, ID (United States), 1992.

[10] J. Ambrosek, Verification and Validation of TMAP7, Tech. Rep., Idaho National Lab.(INL), Idaho Falls, ID (United States), 2008.

[11] J.D. Stempien, R.G. Ballinger, C.W. Forsberg, An integrated model of tritium transport and corrosion in Fluoride Salt-Cooled High-Temperature Reactors (FHRs)–Part I: Theory and benchmarking, Nucl. Eng. Des. 310 (2016) 258–272.

[12] R. Delaporte-Mathurin, E.A. Hodille, J. Mougenot, Y. Charles, C. Grisolia, Finite element analysis of hydrogen retention in ITER plasma facing components using FESTIM, Nucl. Mater. Energy 21 (2019) 100709.

[13] L. Candido, C. Alberghi, Verification and validation of mHIT code over TMAP for hydrogen isotopes transport studies in fusion-relevant environments, Fusion Eng. Des. 172 (2021) 112740.

[14] V. Pasler, F. Arbeiter, C. Klein, D. Klimenko, G. Schlindwein, A. von der Weth, Development and verification of a component-level hydrogen transport model for a DEMO-like HCPB breeder unit with OpenFOAM, Fusion Eng. Des. 127 (2018) 249–258.

[15] F. Urgorri, C. Moreno, E. Carella, D. Rapisarda, I. Fernández-Berceruelo, I. Palermo, A. Ibarra, Tritium transport modeling at system level for the EUROfusion dual coolant lithium-lead breeding blanket, Nucl. Fusion 57 (11) (2017) 116045.

[16] K. Schmid, Diffusion-trapping modelling of hydrogen recycling in tungsten under ELM-like heat loads, Phys. Scr. 2016 (T167) (2016) 014025.

[17] M. Shimada, C. Taylor, Improved tritium retention modeling with reaction-diffusion code TMAP and bulk depth profiling capability, Nucl. Mater. Energy 19 (2019) 273–278.

[18] S. Fukada, R. Anderl, Y. Hatano, S. Schuetz, R. Pawelko, D. Petti, G. Smolik, T. Terai, M. Nishikawa, S. Tanaka, A. Sagara, Initial studies of tritium behavior in flibe and flibe-facing material, Fusion Eng. Des. 61–62 (2002) 783–788.

[19] A.D. Lindsay, TMAP8, 2021, http://dx.doi.org/10.11578/dc.20210205.2.

[20] P.-C.A. Simon, P.W. Humrickhouse, A.D. Lindsay, Tritium transport modeling at the pore scale in ceramic breeder materials using TMAP8, IEEE Trans. Plasma Sci. 50 (11) (2022) 4465–4471.

[21] F. Colliva, F. Hattab, S. Siriano, G. Ferrero, S. Meschini, R. Testoni, M. Zucchetti, A. Iaboni, G.V. Centomani, A. Trotta, C. Ciurluini, Conceptual design and supporting analysis of a double wall heat exchanger for an ARC-class fusion reactor primary cooling system, Fusion Eng. Des. 201 (2024) 114261.

[22] I. Ali-Khan, K. Dietz, F. Waelbroeck, P. Wienhold, The rate of hydrogen release out of clean metallic surfaces, J. Nucl. Mater. 76 (1978) 337–343.

[23] J.D. Stempien, Tritium Transport, Corrosion, and Fuel Performance Modeling in The Fluoride Salt-Cooled High-Temperature Reactor (FHR) (Ph.D. thesis), Massachusetts Institute of Technology, 2015.

[24] A.P. Malinauskas, D.M. Richardson, The solubilities of hydrogen, deuterium, and helium in molten Li2BeF4, Ind. Eng. Chem. Fundam. 13 (3) (1974) 242–245.

[25] F. Waelbroeck, P. Wienhold, J. Winter, E. Rota, T. Bauno, Influence of Bulk and Surface Phenomena on the Hydrogen Permeation Through Metals, Tech. Rep., Kernforschungsanlage Juelich GmbH (Germany, 1984.

[26] A. Pisarev, K. Miyasaka, T. Tanabe, Permeation of hydrogen through tantalum: influence of surface effects, J. Nucl. Mater. 317 (2–3) (2003) 195–203.

[27] C. Greenshields, OpenFOAM v9 User Guide, The OpenFOAM Foundation, London, UK, 2021.

[28] C. Greenshields, H. Weller, Notes on Computational Fluid Dynamics: General Principles, CFD Direct Ltd, Reading, UK, 2022.

[29] S. Fukada, A. Morisaki, Hydrogen permeability through a mixed molten salt of LiF, NaF and KF (Flinak) as a heat-transfer fluid, J. Nucl. Mater. 358 (2–3) (2006) 235–242.

[30] P. Calderoni, P. Sharpe, M. Hara, Y. Oya, Measurement of tritium permeation in flibe (2LiF–BeF2), Fusion Eng. Des. 83 (7–9) (2008) 1331–1334.

[31] R. Macaulay-Newcombe, D. Thompson, W. Smeltzer, Deuterium diffusion, trapping and release in ion-implanted beryllium, Fusion Eng. Des. 18 (1991) 419–424.

[32] H. Carslaw, J. Jaeger, Conduction in Heat and Solids Second Edition, Oxford University Press, 1959, p. 60.

[33] J. Crank, The Mathematics of Diffusion, Oxford University Press, 1979.

[34] A.v.d. Weth, F. Arbeiter, D. Klimenko, V. Pasler, G. Schlindwein, Review of hydrogen isotopes transport parameters and considerations to corresponding experiments, Fusion Eng. Des. 124 (2017) 783–786.

[35] R.A. Causey, R.A. Karnesky, C. San Marchi, Tritium barriers and tritium diffusion in fusion reactors, Compr. Nucl. Mater. 4 (2012) 511–549.

[36] A. Altunoglu, D. Blackburn, N. Braithwaite, D. Grant, Permeation of hydrogen through nickel foils: surface reaction rates at low temperatures, J. Less Common Metals 172–174 (1991) 718–726.

[37] S. Siriano, L. Melchiorri, S. Pignatiello, A. Tassone, A multi-region and a multiphase MHD OpenFOAM solver for fusion reactor analysis, Fusion Eng. Des. 200 (2024) 114216.